

Geophysical Research Letters®



RESEARCH LETTER

10.1029/2023GL104198

Discrete Aurora at Mars: Insights Into the Role of Magnetic Reconnection

Key Points:

- New data confirm that Mars discrete aurora events occur most frequently near strong crustal fields and vary with local time
- Auroral events in adjacent regions with opposite magnetic polarity occur before or after midnight depending on local magnetic field direction
- Magnetic reconnection between crustal fields and the draped interplanetary field appears to control regional and local time behavior

Supporting Information:

Supporting Information may be found in the online version of this article.











Correspondence to:

N. M. Schneider,
nick.schneider@lasp.colorado.edu

Citation:

Johnston, B. J., Schneider, N. M., Jain, S. K., Milby, Z., Deighan, J., Bowers, C. F., et al. (2023). Discrete aurora at Mars: Insights into the role of magnetic reconnection. *Geophysical Research Letters*, 50, e2023GL104198. <https://doi.org/10.1029/2023GL104198>

Received 21 APR 2023
Accepted 18 OCT 2023

B. J. Johnston¹, N. M. Schneider¹ , S. K. Jain¹ , Z. Milby², J. Deighan¹ , C. F. Bowers^{3,4} , G. A. DiBraccio⁵ , J.-C. Gérard⁶, L. Soret⁶ , Z. Girazian⁷ , D. A. Brain¹ , S. Ruhunusiri⁷ , and S. Curry⁸ 

¹Laboratory for Atmospheric and Space Physics, University of Colorado at Boulder, Boulder, CO, USA, ²Division of Geological and Planetary Sciences, California Institute of Technology, Pasadena, CA, USA, ³Department of Climatology and Space Physics, University of Michigan, Ann Arbor, MI, USA, ⁴Dublin Institute for Advanced Studies, Climatology and Space Sciences and Engineering, Dublin, Ireland, ⁵Goddard Space Flight Center, Greenbelt, MD, USA, ⁶LPAP, STAR Institute, University of Liège, Liège, Belgium, ⁷University of Iowa, Iowa City, IA, USA, ⁸Space Sciences Lab, University of California at Berkeley, Berkeley, CA, USA

Abstract Discrete aurora are sporadic emissions of light originating in Mars upper atmosphere. We report nadir imaging observations from MAVEN's Imaging UltraViolet Spectrograph which identify the conditions which trigger electron precipitation causing these events. Prior studies have shown that discrete aurora events in the strong crustal magnetic field region in the southern hemisphere are the brightest and most repeatable compared to events occurring outside the region. Our new data set offers a more complete and accurate characterization of aurora in this area. The region of strongest crustal fields is composed of two distinct magnetic regions, with magnetic fields in opposite directions; discrete aurora events trigger in one region after dusk and in the other before dawn. Magnetic reconnection in these two adjacent regions with the draped interplanetary field may open the crustal fields in these regions during opposing local times. Particle precipitation can then cause discrete aurora at the observed times and locations.

Plain Language Summary Mars has a surprising variety of types of aurora, all different from Earth's "northern lights." Mars lacks the familiar high-latitude aurora because it no longer has the same kind of global magnetic field Earth does. This study examines "discrete aurora" events that occur in region in Mars southern hemisphere that has retained some of the ancient magnetic field. It takes the form of long arcades of magnetic loops that resemble a set of arches. As Mars rotates, these arcades are carried around the planet as the solar wind and its imbedded magnetic field are carried past the planet. We show that when conditions are favorable, the magnetic field locked in the solar wind can interact and "reconnect" with Mars magnetic loops, allowing energetic particles to spiral down the field lines into the atmosphere to cause discrete aurora.

1. Introduction

Discrete aurora events on Mars are sporadic and localized emissions occurring on the nightside portion of the planet in the mid-ultraviolet (MUV), far-ultraviolet, and possibly visible regions of the spectrum. The phenomenon was first identified in MUV emissions by the SPICAM ultraviolet spectrograph on the Mars Express spacecraft (Bertaux et al., 2005). Subsequent studies (Gérard et al., 2015; Leblanc et al., 2006; Soret et al., 2016) further characterized the phenomenon and expanded the list of detections to 19 in total. Detections clustered around a region in Mars' southern hemisphere where the strongest magnetic fields are present (Acuna et al., 1999). Analysis of these SPICAM auroral detections with contemporaneous precipitating electron population measurements (Brain et al., 2006; Gérard et al., 2015; Halekas et al., 2008; Leblanc et al., 2008; Lundin et al., 2006) revealed that discrete aurora are caused by 40–200 eV electrons depositing their energy near 130 km altitude (Leblanc et al., 2006; Soret et al., 2016).

A new wave of observations was enabled by the arrival of the MAVEN spacecraft at Mars in 2014 (Jakosky et al., 2014) carrying the Imaging UltraViolet Spectrograph (IUVS, McClintock et al., 2015). IUVS observations discovered two additional types of aurora which occur globally: diffuse aurora, caused by solar energetic particle storms (Schneider et al., 2015a, 2015b, 2018) and dayside proton aurora, caused by solar wind protons interacting with Mars' hydrogen corona (Deighan et al., 2018). In addition to these planet-wide phenomena, IUVS made its first detection of localized discrete aurora in nadir imaging during a space weather event (Schneider et al., 2018).

© 2023. The Authors.

This is an open access article under the terms of the [Creative Commons Attribution-NonCommercial-NoDerivs License](https://creativecommons.org/licenses/by/4.0/), which permits use and distribution in any medium, provided the original work is properly cited, the use is non-commercial and no modifications or adaptations are made.

MAVEN/IUVS also made extensive limb scan observations of discrete aurora. Schneider et al. (2021), hereafter Schneider21, undertook a deep study of 7 years of limb scan observations, identifying 363 detections and carrying out a number of statistical analyses to understand the cause of the phenomenon. A companion study (Soret et al., 2021) analyzed the vertical profiles and spectra. Schneider21 identified three parameters which control the detection frequency for discrete aurora:

1. Auroral events are brightest and occur most frequently near the strongest crustal fields.
2. Events near strong crustal fields occur most frequently before midnight.
3. Events occur most frequently when the interplanetary magnetic field (IMF) carried by the solar wind is oriented in the dawnward direction across the planet.

Taken together, these three criteria pointed the way toward understanding the triggering mechanism, which must be controlled by a combination of geographic location on Mars (proximity to strong crustal fields), solar wind conditions (IMF direction) and favorable geometry (local time). This combination of factors suggests that discrete aurora result from electron precipitation on open magnetic field lines connecting the crustal fields to the draped solar wind, and that the likelihood of open topology varies for each location with local time and crustal field orientation. In particular, open magnetic topology has been demonstrated to depend on local crustal magnetic field orientations, which vary considerably on scales of hundreds of km within the crustal field regions (Brain et al., 2003). Fang et al. (2022) opened a new line of discrete aurora analysis using 3D magnetohydrodynamic modeling to predict conditions under which precipitation would occur.

Girazian et al. (2022) analyzed correlations between the IMF orientation and discrete aurora detection frequency with two key findings:

1. Events are more common during high solar wind pressure.
2. Events are rare for near radial IMF conditions in the strong crustal field region.

The limb scan data set proved inadequate to identify different regional behaviors of discrete aurora. Despite extensive and regular nightside observations, limb scan studies were limited in observational coverage, subject to observational biases and hampered by line-of-sight location accuracy. Each periapse sampled a relatively narrow swath along the limb, restricted to looking perpendicular to spacecraft motion. Periapse latitude and local time evolved as the orbit precess, giving non-uniform data coverage over the nightside and no data when periapse fell on the dayside.

Line-of-sight ambiguities intrinsic to limb observations prevented unique geographic location determination of the emissions. The patchy nature of discrete aurora emissions exacerbated the problem: emissions patches could be in front of or behind the limb tangent point, with no way to distinguish between them. In the end, geographic locations for most observations were uncertain to hundreds of km. Given the complex magnetic field structure, this ambiguity prevented any identification of even the local field direction in the emitting region. A different observational tool was required to take the next step in understanding the local time triggering of discrete aurora.

Nadir imaging of discrete aurora offers an orthogonal perspective to address the shortcomings of limb observations. Global imaging captures a much larger fraction of the nightside in each orbit, increasing geographic and local time coverage and thereby reducing observational bias. Emission locations in nadir observations are limited by pixel resolution and are unaffected by line-of-sight ambiguities. (These benefits come at the expense of vertical resolution possible with limb scans, which makes the two data sets quite complementary.) Schneider et al. (2018) first demonstrated the feasibility of nadir imaging through the detection of MUV emissions from multiple auroral features in a single image spanning Mars' nightside. The EMUS instrument aboard the Emirates Mars Mission used its high-sensitivity FUV imager to map frequent discrete aurora in the strong crustal field region, and discovered additional morphological features not tied to crustal fields (Lillis et al., 2022).

This study returns to the IUVS nadir imaging methodology of Schneider et al. (2018) with the goal of identifying a sufficient sample of discrete auroral detections in order to shed new light on the identification of the auroral triggering mechanism, specifically searching for regional control. In Section 2 we describe the methodology which enables the detection of nearly 200 new auroral events. In Section 3 we show how the new data set extends and clarifies local time control, and identifies local magnetic field direction as the critical variable. In Section 4 we offer a working hypothesis for reconnection which is consistent with all the known controlling factors for triggering. Section 5 places this working hypothesis in the broader context and suggests avenues of future work.

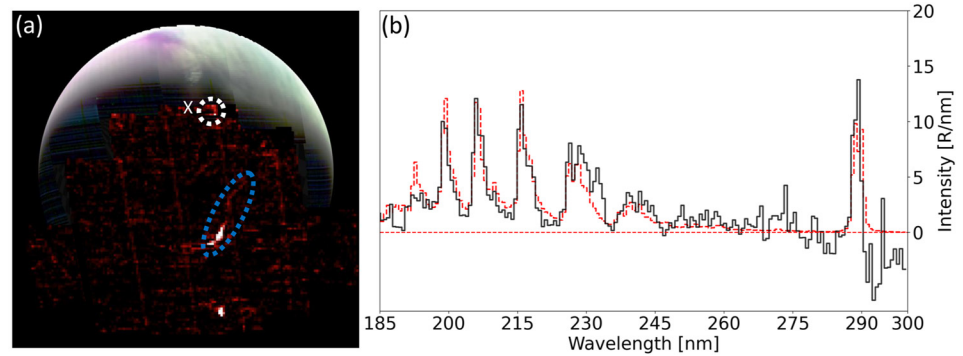


Figure 1. (a) Nadir image showing a global view of Mars on orbit 3134, with multiple discrete auroral emissions. The dayside portion of the planet is visible on the upper third of the image above the terminator. The blue ellipse locates a verified discrete auroral emission with a Pearson-R coefficient of 0.8. The white ellipse locates an instrument artifact, with a Pearson-R correlation coefficient of 0.2. (b) The black line shows the average spectrum of the 30 bright pixels making up the bright “string bean” feature circled in blue. The red dashed line shows the spectral fit of auroral emissions to the data, with fitted solar continuum spectrum and constant background removed. Deviations between the observed average spectrum and the fit are not considered statistically significant given low signal levels. The region from 250 to 270 nm contains no auroral emissions and indicates what a non-auroral spectrum looks like.

Building on these results, the companion paper by Bowers et al. (2023), hereafter Bowers23, examines the working hypothesis of magnetic reconnection in the context of MAVEN measurements of magnetospheric and solar wind properties.

2. Observations

The IUVS instrument obtains nadir observations during the ~1 hr-long apoapse segment of MAVEN's ~5 hr elliptical orbit (e.g., Connour et al., 2020). The spectrograph slit is 10° long and scans perpendicular to spacecraft orbital motion. The combination of spacecraft motion and perpendicular slit scanning allows IUVS to build full multispectral disk images of Mars, covering both night and day sides. The high-voltage intensifier gain is increased for higher sensitivity during nightside observations. At the nadir point, a spatial pixel subtends ~55 km. Detector images are binned to cover the MUV range from ~185 to 325 nm using either 256 or 512 spectral bins, meaning that each spatial pixel along the slit has a corresponding MUV spectrum. The data processing and methodology below follows that used by Schneider et al. (2020) for the study of nitric oxide nightglow in the same data set of nightside observations. As in that work, each spatial pixel holds a complete MUV spectrum suitable for fitting, correction and further analysis. Only pixels at solar zenith angles >102° were considered, as multiple scattering from martian clouds and dust contaminates the nightside spectrum with dayside solar continuum. Beyond this angle, the solar continuum component can be reliably fitted and subtracted.

Nadir-viewing nightside data from MAVEN orbits 3000 to 14500 (April 2016 to August 2021) were evaluated for discrete auroral emissions. Each nightside image was obtained in multiple swaths using scan mirror motion. Only swaths with at least 30 nightside spatial elements in the scan direction were used in the study, necessary to obtain sufficient pixels away from the limb of the planet and to characterize the image background levels. Swaths from 5,896 different orbits met this criterion for further analysis. 1,296 orbits had suitable viewing geometry for full coverage of the strong crustal field region on the nightside.

Discrete aurora appear as bright, localized, and spatially-coherent features across the nightside disk. Figure 1a shows a nadir image taken by IUVS with a confirmed auroral detection circled in blue, and its associated spectrum shown in Figure 1b. Detections from this data set were identified manually pixel-by-pixel, and each summed spectrum from these pixels was individually confirmed through spectral analysis. No magnetic field or geographic location information was used to distinguish auroral detections from dayside emissions or instrument artifacts. Features with five or more spatially-adjacent pixels containing verified auroral signatures were summed to produce a single spectrum to evaluate for a confirmed detection. As in Schneider21, a Pearson-R correlation was performed between a discrete aurora spectral template and the summed spectrum for each detection; detections with correlation coefficients greater than 0.6 were considered genuine (Figure 1b). Due to the global coverage of the disk, a single orbit could contain multiple spatially distinct auroral detections.

Detection locations were initially mapped to the line-of-sight surface intercept and then corrected for viewing geometry. The emissions were assumed to lie at 135 km emission altitude as measured in limb scans (Soret et al., 2021). Surface intercepts corrections ranged from 0 km at nadir to ~580 km for ~80° emission angle, with an average correction value of 200 km for all detections.

3. Results

A total of 126 discrete auroral detections were identified, with 50 detections (40%) within the strong crustal field region defined in Schneider21 (150°–210°E, 30°–60°S). Each detection consisted of 5–55 pixels, spanning ~45–135 km in width and ~120–1,500 km in length. The narrowest features filled only a single spatial pixel in width, and therefore can only be considered upper limits on the widths. These values are in agreement with the spatial extents between 21 and 125 km and mean value of 44 km observed with SPICAM at the nadir (Gérard et al., 2015). Brightnesses, uncertainties, latitudes, longitudes, local times, solar zenith angles and other observation properties were tabulated for individual pixels and for summed events, along with solar wind and IMF conditions. Cameron band emission brightnesses ranged from 0.5 to 2.6 kR. Table 1 in Supporting Information S1 contains the derived properties of each detection, and the specially-processed data files from which they were extracted are available at the CU Scholar repository (Jain & Schneider, 2023).

Detections occur globally, however detections near the strong crustal field region show high repeatability in emission location. Figure 2a shows a global map of Mars with each discrete auroral detection overplotted using a rainbow colorbar corresponding to orbit number. Figure 2b zooms in around the strong crustal field region. The variety of overlapping colors in the localized regions is strong evidence of the repeatability of events in the same locations over the years of observation.

Detections in the strong crustal field region show the same preference for occurring during the dawnward-pointing IMF orientation as seen in the limb scan analysis of Schneider21 and Girazian et al. (2022). (Dawnward is equivalent to $-B_y$ often used in the literature.) Solar wind proxies developed by Ruhunusiri et al. (2018) were used to determine the IMF conditions for these detections because MAVEN did not have sufficient solar wind coverage during the IUVS nadir observations. Although there are several detections that occur during the dusk-pointing IMF orientation, detections in the strong crustal field region are ~5 times more likely to occur for the dawnward-pointing IMF orientation. IMF correlations with nadir discrete aurora detections for this study are shown in Bowers23.

Figure 3a shows detections in the strong field region color-coded by local time, clearly demarcating a northern region where auroral events occur before midnight and a southern region where they occur after midnight. (The bounding box used here differs slightly from that in Schneider21, as explained below.) Analysis of local time occurrence frequency histograms clearly show two regions which trigger at opposing local times: the northern region (approximately -37° to -52° latitude, 156° – 211° longitude) triggers pre-midnight peaking near the early evening hours around 20hr local time, and the southern region (approximately -52° to -68° latitude, 156° – 211° longitude) triggers post-midnight peaking before dawn around 6 hr local time. There are 41 individual auroral events occurring in the northern region and 18 occurring in the southern region. The clear 1° (60 km) separation between pre- and post-midnight discrete aurora detection locations at -52° latitude is an indication that the responsible physical process has a spatial scale of ~60 km or less.

The identification of regions triggering before and after midnight improves upon the local time characterization in the limb scan data set of Schneider21. They found the strong tendency for pre-midnight aurora in a box encircling their highest density of detections, but did not detect the post-midnight trend seen at southern latitudes in Figure 3a. The primary reason is that the Schneider21 box only extended to -60° latitude where limb scans detections declined, such that the active region along -65° latitude was excluded and half of the potential detections were eliminated. A reanalysis of the limb scan data set in light of the current work confirms that the southern region triggering after midnight is detectable using improved geographic limits, albeit at smaller number statistics.

Figure 3b shows the strength and direction of crustal fields in the strong crustal field region. This region of crustal magnetism shows that the northern and southern regions are magnetically distinct, each spanning $\sim 30^\circ$ longitude and $\sim 17^\circ$ latitude with opposite local field polarity. Figure 3b shows a 3D cartoon representing field lines connecting positive vertical fields to negative fields as yellow arrows, following the local crustal field orientation

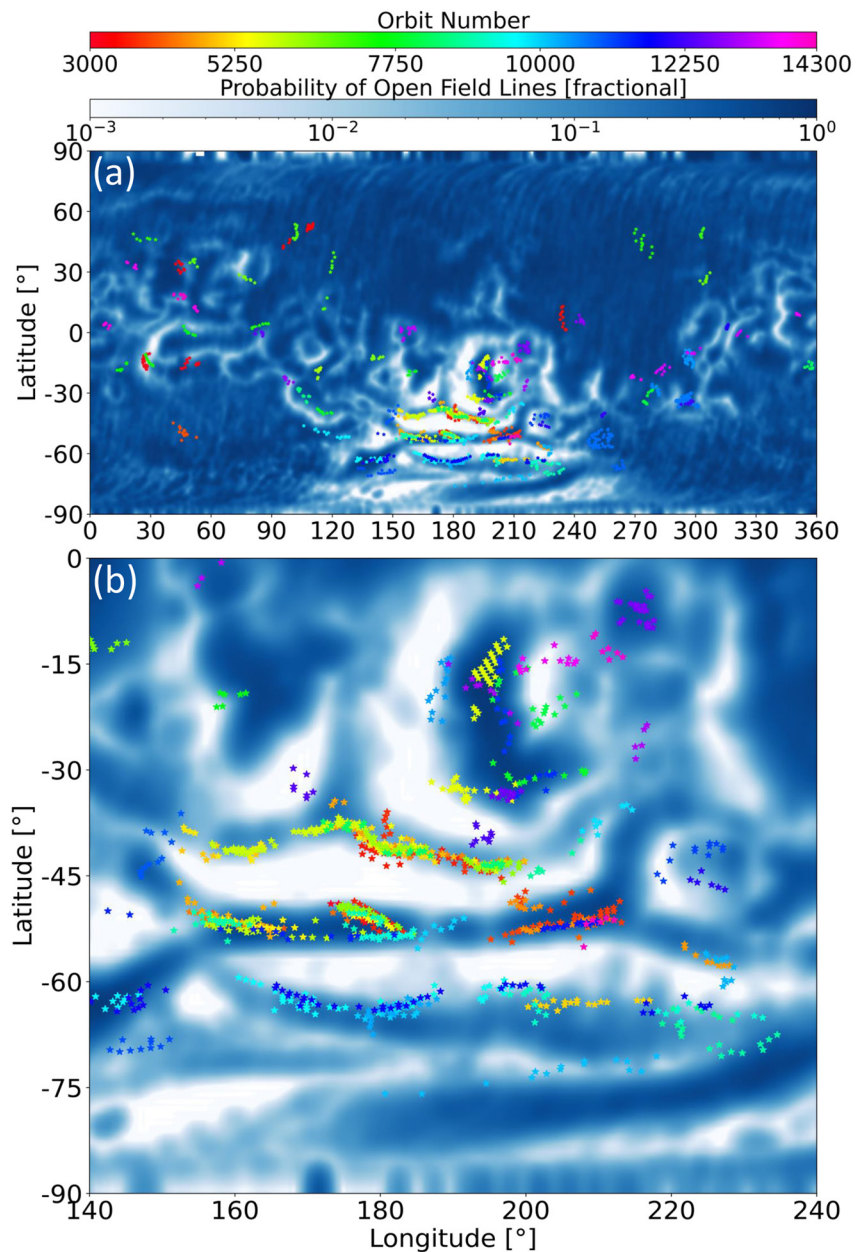


Figure 2. Magnetic field map of Mars with overplotted discrete auroral detections. The blue-white color scale indicates the fractional probability of open magnetic field lines, with dark blue locations containing the highest probability of open field lines (Brain et al., 2007). Mean latitude and longitude auroral emission detection locations are overplotted and color-coded by orbit number. Note that some detections are hidden because they are overplotted by separate detections occurring in nearly identical locations on different orbits. (a) Global view of Mars with all detections overplotted. (b) Zoomed-in version showing detections in the strong crustal field region nicknamed “the sailboat.”

and strength. Discrete auroral emissions are detected above the footprints of these loops where the magnetic field lines terminate in the crust of the planet. The southern loop of crustal magnetism closes to the south, and discrete auroral activity is detected when this loop is in the post-midnight sector, primarily near the dawn terminator. The northern loop of crustal magnetism closes to the north, and discrete auroral activity is detected in this region when the loop is in the pre-midnight sector, and primarily near the dusk terminator. The region near 52°S latitude where the southern and northern loops meet activate for both dusk and dawn geometries on their respective sides of the dividing line evident in Figure 3.

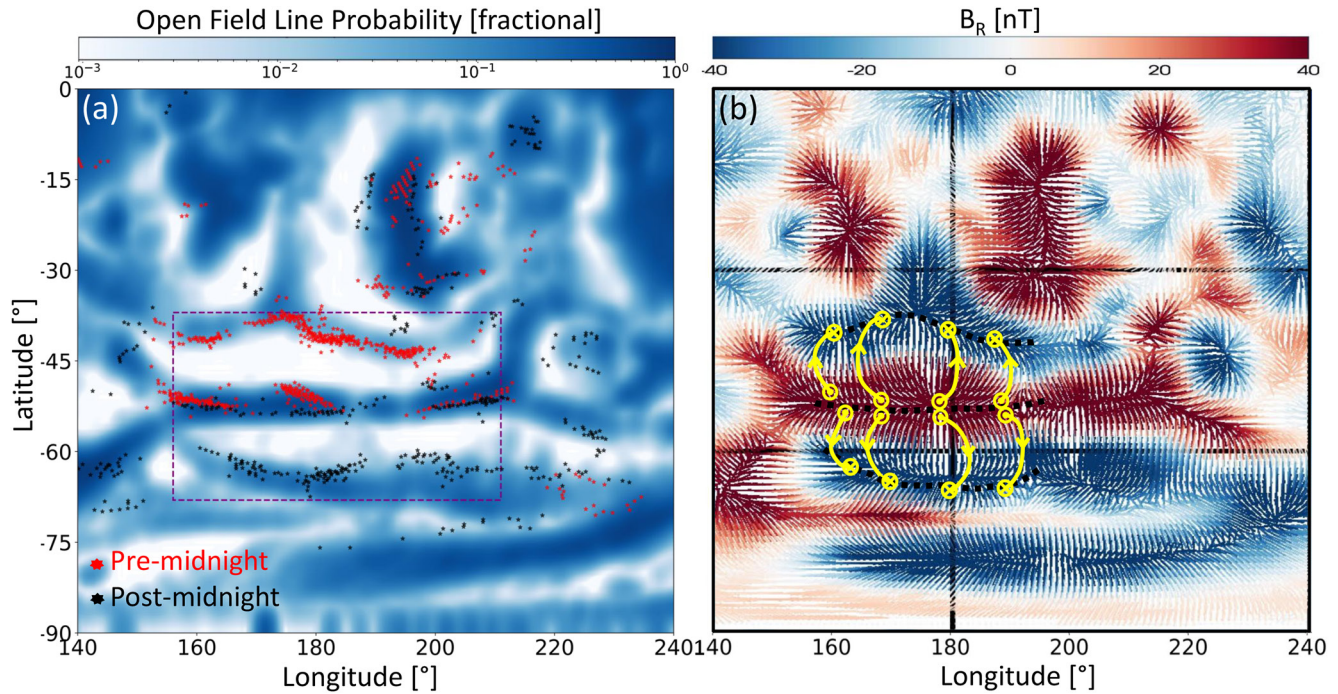


Figure 3. (a) Mean detection locations color-coded by local time overlaid on a martian magnetic field probability map as in Figure 2. There are two distinct groupings adjacent to each other but triggering at distinct local times. Pre-midnight detections are shown in red and post-midnight detections are shown in black. This study defines a rectangular box (shown in purple) delineating the strong crustal field region (156° – 211° E, 37° – 68° S). (b) Whisker plot showing crustal field strength and direction from Brain et al. (2003) with overlaid crustal field “arcades” (yellow loops). The red-blue arrows in this plot signify crustal field strength and direction, with red arrows indicating positive ($+r$) radial crustal fields and blue arrows indicating negative ($-r$) radial crustal fields. The northern arcade corresponds to northerly horizontal magnetic fields, and the south arcade to the southerly horizontal magnetic fields.

4. Discussion

Here, we present magnetic reconnection as a working hypothesis to explain this observed local time dependence of auroral emissions within the strong crustal field region. Reconnection is known to operate at Earth (e.g., Phan et al., 2010), was recently detected at Ganymede (Ebert et al., 2022) and likely occurs many other places in the solar system. In this process, magnetic fields lines reconfigure and transfer energy into the surrounding environment, mixing previously separate plasma populations. This process “opens up” the closed magnetic loops of the crustal anomalies and allows electrons to precipitate along the new field lines until they ultimately collide with the atmosphere, producing auroral emissions over regions where the newly-open magnetic fields intersect the planet’s surface. Magnetic fields are more susceptible to reconnection when a large (nearly anti-parallel) shear angle (the angle between the draped IMF and local crustal magnetic field) is present (Gosling & Phan, 2013; Bowers23). Specifically for this scenario, large angles between the magnetic field vectors of the crustal fields and draped IMF present an opportunity for reconnection to occur. Therefore, we expect the local draped IMF orientation to affect the location of discrete auroral emissions.

Fang et al. (2018) applied a global magnetohydrodynamic model toward understanding the variations in the IMF orientation as it drapes around the planet. Their results showed that an IMF field line oriented in the plane orthogonal to the flow of the solar wind (i.e., the Y_{MSO} direction) will bend away from that plane as it drapes around the planet and exhibit significant asymmetries around the dawn/dusk terminators (see Figure 1 of their study). This draping pattern shows that, in the southern hemisphere, a $-B_{y,\text{MSO}}$ IMF field line would shift toward the $+Z_{\text{MSO}}$ direction (northward) on the dawn terminator (post-midnight sector) and in the $-Z_{\text{MSO}}$ direction (southward) on the dusk terminator (pre-midnight sector). This draping pattern was also demonstrated using MAVEN magnetometer data in Chai et al. (2019) and Dubinin et al. (2019).

Figure 4 demonstrates how this draped magnetic field configuration from Fang et al. (2018) would appear from the dawn side, dayside, and dusk side of the planet, with the strong crustal field region of interest located at 06:00, 12:00, and 18:00 hr local time, respectively. On the dayside of the planet, the draped IMF is at a low shear angle

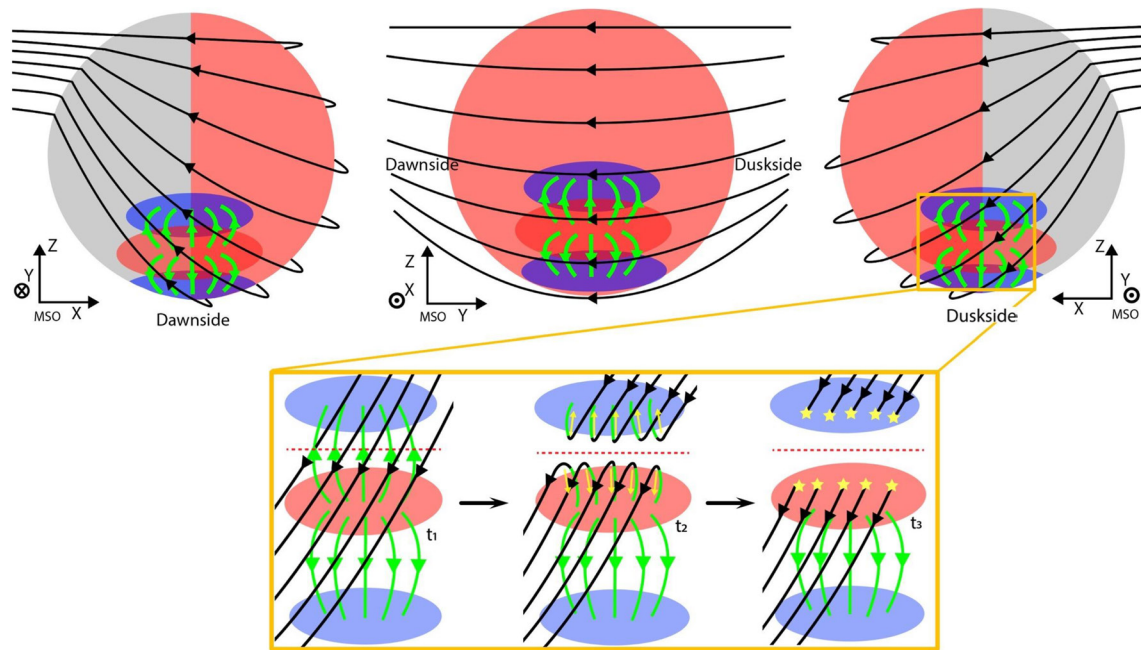


Figure 4. The top panel shows the draping pattern of an upstream $-B_y$ interplanetary magnetic field (IMF) field line (black arrow) around Mars as seen from three perspectives. The crustal fields are enlarged for clarity, with blue/red ovals representing radially inward/outward magnetic fields. The transverse component of the crustal magnetic fields is shown in green. On the left in the bottom panel, reconnection is likely where the IMF in black is more anti-parallel to the crustal field in green. Yellow stars in the bottom right panel show where open field lines will allow particle precipitation and aurora in the northern arcade at dusk.

($\sim 90^\circ$) to the crustal field region and is therefore unlikely to undergo reconnection. On the dusk side, a southward shifted draped IMF creates a large shear with the northern crustal loop, making it more likely for reconnection to occur in this region and, therefore, more likely for the activation of auroral emissions. This process is shown in the zoom-in box of Figure 4. On the dawn side, large shear occurs in the southern arcade and reconnection is likely here (see Bowers23 for supporting figures).

While this work makes the case that magnetic reconnection is a precursor to auroral events, it offers no immediate insights into the subsequent processes or mechanisms. The analysis at present does not distinguish whether reconnection itself triggers particle acceleration, or allows potential structures to arise which accelerate precipitating particles, or merely opens up a path for existing electron populations to reach the atmosphere. Bowers23 provides a more rigorous analysis to address the hypothesis that magnetic reconnection is responsible for discrete aurora formation.

5. Summary and Future Work

This study builds on recent limb scan analyses (Schneider21; Soret et al., 2021), using nadir imaging to add better spatial accuracy and resolution, local time coverage and geographic coverage. The result is a more complete characterization of the locations, timing and conditions for discrete aurora events. The new results confirm the prior characterization in terms of geographic distribution, and correlations with magnetic field strength, local time and IMF direction. Going further, this work takes advantage of the nadir viewing geometry to undertake a regional study of aurora in the heart of the strong crustal field region.

The most dramatic result of this work is the clear delineation of two magnetic arcades of opposite north/south polarity, one of which triggers aurora before midnight and the other after (Figure 3a). Past work (e.g., Fang et al. (2018) has shown that the draped interplanetary field has opposing north/south components at these two local times, making one arcade more susceptible to reconnection before midnight and the other after midnight (Figure 4). While this argument is fundamentally geometric in nature, the more rigorous approach in Bowers23 reaches the same conclusion. We emphasize that we conclude only that magnetic reconnection is a likely precursor to discrete aurora events, without immediate insights into the exact mechanisms.

These results open several new avenues for future study. First, the IUVS nadir data coverage includes a number of additional magnetic domains that may exhibit distinct local time behaviors. For example, Figure 3 hints at differences in local time occurrences elsewhere in the “sailboat” region (Figure 3a) where the horizontal fields differ substantially from those in this work. Second, Mars' changing seasonal tilt should affect the probability of reconnection, as the arcade horizontal fields rock ± 25 degrees relative to the draped IMF, and a follow-on study should be able to test this hypothesis. Given the high southern latitudes of the strong crustal field region, however, it may be challenging to get uniform coverage at the critical time of greatest tilt in southern summer. Third, the rich data set on discrete aurora in the strong crustal field region from the EMUS instrument on the EMM mission (Lillis et al., 2022) would benefit from the local time and seasonal analyses described above. This work would benefit from MAVEN in situ data contemporaneous with EMUS observations. Finally, MAVEN's particles and fields data sets could be further analyzed in the framework of the reconnection hypothesis, as outlined in Bowers23. In fact, the \sim twice-daily recurrence of magnetic reconnection in repeatable locations might offer future orbital missions the easiest access to limited regions where this fundamental magnetospheric process occurs.

Data Availability Statement

In accordance with the AGU data policy, the data used in this study may be obtained from the Planetary Atmospheres Node of the Planetary Data System at <https://atmos.nmsu.edu/PDS/data/PDS4/MAVEN/> using the file names containing the keyword “apoapse” and version “v13.” Special data products produced for this work are available at the CU Scholar repository (Jain & Schneider, 2023).

Acknowledgments

The MAVEN mission is supported by NASA in association with the University of Colorado and NASA's Goddard Space Flight Center. JCG and LS acknowledge support from the Belgian Federal Science Policy Office, with financial and contractual coordination by the ESA PRODEX Office (PEA Grant 4000140863).

References

- Acuna, M. H., Connerney, J. E., Ness, N. F., Lin, R. P., Mitchell, D., Carlson, C. W., et al. (1999). Global distribution of crustal magnetization discovered by the Mars Global Surveyor MAG/ER experiment. *Science*, 284(5415), 790–793. <https://doi.org/10.1126/science.284.5415.790>
- Bertaux, J.-L., Leblanc, F., Witasse, O., Quemerais, E., Lilensten, J., Stern, S. A., et al. (2005). Discovery of an aurora on Mars. *Nature*, 435(7043), 790–794. <https://doi.org/10.1038/nature03603>
- Bowers, C. F., DiBraccio, G. A., Slavin, J. A., Johnston, B., Schneider, N. M., Brain, D. A., & Azari, A. (2023). Exploring magnetic reconnection as the precursor to discrete aurora at Mars. *Journal of Geophysical Research: Space Physics*. <https://doi.org/10.1029/2023JA01622>
- Brain, D. A., Bagenal, F., Acuña, M. H., & Connerney, J. E. P. (2003). Martian magnetic morphology: Contributions from the solar wind and crust. *Journal of Geophysical Research*, 108, A12. <https://doi.org/10.1029/2002JA009482>
- Brain, D. A., Halekas, J. S., Peticolas, L. M., Lin, R. P., Luhmann, J. G., Mitchell, D. L., et al. (2006). On the origin of aurorae on Mars. *Geophysical Research Letters*, 33(1), 01201. <https://doi.org/10.1029/2005GL024782>
- Brain, D. A., Lillis, R. J., Mitchell, D. L., Halekas, J. S., & Lin, R. P. (2007). Electron pitch angle distributions as indicators of magnetic field topology near Mars. *Journal of Geophysical Research*, 112(A9), A09201. <https://doi.org/10.1029/2007JA012435>
- Chai, L., Wan, W., Wei, Y., Zhang, T., Exner, W., Fraenz, M., et al. (2019). The induced global looping magnetic field on Mars. *The Astrophysical Journal Letters*, 871(2), L27. <https://doi.org/10.3847/2041-8213/aaff6e>
- Connour, K., Schneider, N. M., Milby, Z., Forget, F., Alhosani, M., Spiga, A., et al. (2020). Mars' twilight cloud band: A new cloud feature seen during the 2018 global dust storm. *Geophysical Research Letters*, 47(1), e2019GL084997. <https://doi.org/10.1029/2019GL084997>
- Deighan, J., Jain, S. K., Chaffin, M. S., Fang, X., Halekas, J. S., Clarke, J. T., et al. (2018). Discovery of proton aurora at Mars. *Nature Astronomy*, 2(10), 802–807. <https://doi.org/10.1038/s41550-018-0538-5>
- Dubinin, E., Modolo, R., Fraenz, M., Pätzold, M., Woch, J., Chai, L., et al. (2019). The induced magnetosphere of Mars: Asymmetrical topology of the magnetic field lines. *Geophysical Research Letters*, 46(22), 12722–12730. <https://doi.org/10.1029/2019GL084387>
- Ebert, R. W., Fuselier, S. A., Allegrini, F., Bagenal, F., Bolton, S. J., Clark, G., et al. (2022). Evidence for magnetic reconnection at Ganymede's upstream magnetopause during the PJ34 Juno flyby. *Geophysical Research Letters*, 49(23), e2022GL099775. <https://doi.org/10.1029/2022GL099775>
- Fang, X., Ma, Y., Luhmann, J., Dong, Y., Brain, D., Hurley, D., et al. (2018). The morphology of the solar wind magnetic field draping on the dayside of Mars and its variability. *Geophysical Research Letters*, 45(8), 3356–3365. <https://doi.org/10.1002/2018GL077230>
- Fang, X., Ma, Y., Schneider, N., Girazian, Z., Luhmann, J., Milby, Z., et al. (2022). Discrete aurora on the nightside of Mars: Occurrence location and probability. *Journal of Geophysical Research: Space Physics*, 127(3), e2021JA029716. <https://doi.org/10.1029/2021JA029716>
- Gérard, J.-C., Soret, L., Libert, L., Lundin, R., Stiepen, A., Radioti, A., & Bertaux, J. (2015). Concurrent observations of ultraviolet aurora and energetic electron precipitation with Mars Express. *Journal of Geophysical Research*, 120(8), 6749–6765. <https://doi.org/10.1002/2015JA021150>
- Girazian, Z., Schneider, N. M., Milby, Z., Fang, X., Halekas, J., Weber, T., et al. (2022). Discrete aurora at Mars: Dependence on upstream solar wind conditions. *Journal of Geophysical Research: Space Physics*, 127(4), e2021JA030238. <https://doi.org/10.1029/2021JA030238>
- Gosling, J. T., & Phan, T. D. (2013). Magnetic reconnection in the solar wind at current sheets associated with extremely small field shear angles. *The Astrophysical Journal*, 763(2), L39. <https://doi.org/10.1088/2041-8205/763/2/L39>
- Halekas, J. S., Brain, D. A., Lin, R. P., Luhmann, J. G., & Mitchell, D. L. (2008). Distribution and variability of accelerated electrons at Mars. *Advances in Space Research*, 41(9), 1347–1352. <https://doi.org/10.1016/j.asr.2007.01.034>
- Jain, S., & Schneider, N. M. (2023). Discrete aurora at Mars: Insights into the Role of magnetic reconnection [Dataset]. University of Colorado Boulder. <https://doi.org/10.25810/23D5-A443>
- Jakosky, B., Lin, R. P., Grebowsky, J. M., Luhmann, J. G., Mitchell, D. F., Beutelschies, G., et al. (2014). The 2013 Mars atmosphere and volatile evolution (MAVEN) mission to Mars. *Space Science Reviews*, 195(1–4), 3–48. <https://doi.org/10.1007/s11214-015-0139-x>
- Leblanc, F., Witasse, O., Lilensten, J., Frahm, R. A., Safaenili, A., Brain, D. A., et al. (2008). Observations of aurorae by SPICAM ultra-violet spectrograph on board Mars Express: Simultaneous ASPERA-3 and MARSIS measurements. *Journal of Geophysical Research*, 113, A08311. <https://doi.org/10.1029/2008JA013033>

- Leblanc, F., Witasse, O., Winningham, J., Brain, D., Liliensten, J., Bletty, P.-L., et al. (2006). Origins of the Martian aurora observed by spectroscopy for investigation of characteristics of the atmosphere of Mars (SPICAM) on board Mars express. *Journal of Geophysical Research*, *111*, A09313. <https://doi.org/10.1029/2006JA011763>
- Lillis, R. J., Deighan, J., Brain, D., Fillingim, M., Jain, S., Chaffin, M., et al. (2022). First synoptic images of FUV discrete aurora at Mars by EMM EMUS. *Geophysical Research Letters*, *49*(16), e2022GL099820. <https://doi.org/10.1029/2022GL099820>
- Lundin, R., Winningham, D., Barabash, S., Frahm, R., Holmström, M., Sauvaud, J.-A., et al. (2006). Plasma acceleration above Martian magnetic anomalies. *Science*, *311*(5763), 980–983. <https://doi.org/10.1126/science.112207>
- McClintock, W. E., Schneider, N. M., Holsclaw, G. M., Hoskins, A. C., Stewart, I., Deighan, J., et al. (2015). The imaging ultraviolet spectrograph (IUVS) for the MAVEN mission. *Space Science Reviews*, *195*(1–4), 75–124. <https://doi.org/10.1007/s11214-014-0098-7>
- Phan, T., Gosling, J., Paschmann, G., Pasma, C., Drake, J., Øieroset, M., et al. (2010). The dependence of magnetic reconnection on plasma β and magnetic shear: Evidence from solar wind observations. *The Astrophysical Journal Letters*, *719*(2), L199–L203. <https://doi.org/10.1088/2041-8205/719/2/L199>
- Ruhunusiri, S., Halekas, J. S., Espley, J. R., Eparvier, F., Brain, D., Mazelle, C., et al. (2018). An artificial neural network for inferring solar wind proxies at Mars. *Geophysical Research Letters*, *45*(20), 10855–10865. <https://doi.org/10.1029/2018GL079282>
- Schneider, N. M., Deighan, J. I., Jain, S. K., Stiepen, A., Stewart, A. I. F., Larson, D., et al. (2015a). Discovery of diffuse aurora on Mars. *Science*, *350*(6261). <https://doi.org/10.1126/science.aad0313>
- Schneider, N. M., Deighan, J. I., Stewart, A. I. F., McClintock, W. E., Jain, S. K., Chaffin, M. S., et al. (2015b). MAVEN IUVS observations of the aftermath of the Comet Siding Spring meteor shower on Mars. *Geophysical Research Letters*, *42*(12), 4755–4761. <https://doi.org/10.1002/2015GL063863>
- Schneider, N. M., Jain, S. K., Deighan, J., Nasr, C. R., Brain, D. A., Larson, D., et al. (2018). Global aurora on Mars during the September 2017 space weather event. *Geophysical Research Letters*, *45*(15), 7391–7398. <https://doi.org/10.1029/2018gl077772>
- Schneider, N. M., Milby, Z., Jain, S. K., Gérard, J.-C., Soret, L., Brain, D., et al. (2021). Discrete aurora on Mars: Insights into their distribution and activity from MAVEN/IUVS observations. *Journal of Geophysical Research: Space Physics*, *428*(10), e2021JA029428. <https://doi.org/10.1029/2021JA029428>
- Schneider, N. M., Milby, Z., Jain, S. K., González-Galindo, F., Royer, E., Gérard, J.-C., et al. (2020). Imaging of Martian circulation patterns and atmospheric tides through MAVEN/IUVS nightglow observations. *Journal of Geophysical Research: Space Physics*, *125*(8), e2019JA027318. <https://doi.org/10.1029/2019JA027318>
- Soret, L., Gérard, J.-C., Libert, L., Shematovich, V. I., Bisikalo, D. V., Stiepen, A., & Bertaux, J.-L. (2016). SPICAM observations and modeling of Mars aurorae. *Icarus*, *264*, 398–406. <https://doi.org/10.1016/j.icarus.2015.09.023>
- Soret, L., Gérard, J.-C., Schneider, N., Jain, S., Milby, Z., Ritter, B., et al. (2021). Discrete aurora on Mars: Spectral properties, vertical profiles, and electron energies. *Journal of Geophysical Research: Space Physics*, *126*(10), e2021JA029495. <https://doi.org/10.1029/2021JA029495>